



## ARCHIVIO ISTITUZIONALE DELLA RICERCA

### Alma Mater Studiorum Università di Bologna Archivio istituzionale della ricerca

Intersystem crossing in the entrance channel of the reaction of O(3P) with pyridine

This is the final peer-reviewed author's accepted manuscript (postprint) of the following publication:

*Published Version:*

Intersystem crossing in the entrance channel of the reaction of O(3P) with pyridine / Recio, Pedro; Alessandrini, Silvia; Vanuzzo, Gianmarco; Pannacci, Giacomo; Baggioli, Alberto; Marchione, Demian; Caracciolo, Adriana; Murray, Vanessa J; Casavecchia, Piergiorgio; Balucani, Nadia; Cavallotti, Carlo; Puzzarini, Cristina; Barone, Vincenzo. - In: NATURE CHEMISTRY. - ISSN 1755-4330. - STAMPA. - 14:12(2022), pp. 1405-1412. [10.1038/s41557-022-01047-3]

This version is available at: <https://hdl.handle.net/11585/918905> since: 2023-02-28

*Published:*

DOI: <http://doi.org/10.1038/s41557-022-01047-3>

*Terms of use:*

Some rights reserved. The terms and conditions for the reuse of this version of the manuscript are specified in the publishing policy. For all terms of use and more information see the publisher's website.

(Article begins on next page)

This item was downloaded from IRIS Università di Bologna (<https://cris.unibo.it/>).  
When citing, please refer to the published version.

This is the final peer-reviewed accepted manuscript of:

P. Recio, S. Alessandrini, G. Vanuzzo, G. Pannacci, A. Baggioli, D. Marchione, A. Caracciolo, V.J. Murray, P. Casavecchia, N. Balucani, C. Cavallotti, C. Puzzarini, V. Barone. Intersystem-Crossing in the Entrance Channel without Heavy Atoms: the reaction of O(<sup>3</sup>P) with pyridine. *Nature Chem.* **14** (2022) 1405

The final published version is available online at:

<https://doi.org/10.1038/s41557-022-01047-3>

#### Terms of use:

Some rights reserved. The terms and conditions for the reuse of this version of the manuscript are specified in the publishing policy. For all terms of use and more information see the publisher's website.

*This item was downloaded from IRIS Università di Bologna (<https://cris.unibo.it/>)*

***When citing, please refer to the published version.***

# Intersystem-Crossing in the Entrance Channel without Heavy Atoms: the reaction of O(<sup>3</sup>P) with pyridine

*Pedro Recio,<sup>1#</sup> Silvia Alessandrini,<sup>2,3#</sup> Gianmarco Vanuzzo,<sup>1</sup> Giacomo Pannacci,<sup>1</sup> Alberto Baggioli,<sup>4</sup> Demian Marchione,<sup>1</sup> Adriana Caracciolo,<sup>1‡</sup> Vanessa J. Murray,<sup>1‡‡</sup> Piergiorgio Casavecchia,<sup>1</sup> Nadia Balucani,<sup>1\*</sup> Carlo Cavallotti,<sup>4\*</sup> Cristina Puzzarini,<sup>3\*</sup> and Vincenzo Barone<sup>2\*</sup>*

<sup>1</sup> Dipartimento di Chimica, Biologia e Biotecnologie, Università degli Studi di Perugia, Via Elce di Sotto 8, I-06123 Perugia, Italy

<sup>2</sup> Scuola Normale Superiore di Pisa, Piazza dei Cavalieri 7, I-56126 Pisa, Italy

<sup>3</sup> Dipartimento di Chimica “Giacomo Ciamician”, University of Bologna, via F. Selmi 2, I-40126 Bologna, Italy

<sup>4</sup> Dipartimento di Chimica, Materiali e Ingegneria Chimica "Giulio Natta", Politecnico di Milano, P.zza Leonardo da Vinci 32, I-20131 Milano, Italy

## Summary

**Two quantum effects can enable reactions to take place at energies below the barrier separating reactants from products: tunneling and intersystem-crossing (ISC) between coupled potential energy surfaces (PESs). Here we show that ISC in the region between the pre-reactive complex and the reaction barrier can control the rate of bimolecular reactions for weakly coupled PESs, even in the absence of heavy atoms. For O(<sup>3</sup>P)+pyridine, a reaction relevant to combustion, astro- and bio-chemistry, crossed-beam experiments indicate that the dominant products are pyrrole and CO, obtained through a spin-forbidden ring-contraction mechanism. The experimental findings are interpreted by high-level quantum-chemical calculations and statistical nonadiabatic computations of branching fractions, in terms of an efficient ISC occurring before the high entrance barrier for O-atom addition to the N-atom lone pair. At low/moderate temperatures, the computed reaction rates prove to be dominated by ISC. We suggest that this mechanism may be more common than expected.**

<sup>#</sup>Both authors contributed equally to this work.

<sup>‡</sup> Department of Aerospace Engineering Sciences, University of Colorado, Boulder, CO 80303-0429 USA.

<sup>‡‡</sup> Montana State University, Bozeman MT, USA.

\*Corresponding authors: Vincenzo Barone ([vincenzo.barone@sns.it](mailto:vincenzo.barone@sns.it)); Nadia Balucani ([nadia.balucani@unipg.it](mailto:nadia.balucani@unipg.it)); Carlo Cavallotti ([carlo.cavallotti@polimi.it](mailto:carlo.cavallotti@polimi.it)); Cristina Puzzarini ([cristina.puzzarini@unibo.it](mailto:cristina.puzzarini@unibo.it))

Classical kinetic theories predict that reaction rates vanish when the energy available to the reactants is lower than the barrier leading to the formation of products.<sup>1</sup> However, quantum effects (such as tunnelling and resonance) can alter the classically expected results, leading to non-Arrhenius behaviours.<sup>2-5</sup> For instance, while the rate coefficients of several bimolecular reactions are expected to become vanishingly small at the low temperature typical of interstellar clouds (as low as 10 K), recent experimental work demonstrated that quantum tunnelling from a weakly bound entrance complex, through the reaction barrier, can strongly affect the reaction rate coefficient with important consequences for the chemistry of that exotic environment.<sup>4,6,7</sup>

Another important quantum effect originates from the nonadiabatic transition between potential energy surfaces (PESs) of two electronic states of different spin multiplicity, also known as intersystem-crossing (ISC).<sup>8-10</sup> Extensive experimental and theoretical studies have shown that, in the unimolecular decomposition of a photoexcited molecule, the occurrence of nonadiabatic transitions at the seam of intersection between PESs of different multiplicity is very common and plays an important role in many environmental, biological, and technological processes.<sup>11,12</sup> ISC can also occur in bimolecular reactions.<sup>8-10,13-23</sup> The presence of heavy atoms (e.g., iodine or transition metals) can strongly enhance the spin-orbit coupling between states of different multiplicity (strongly coupled PESs) and thus increase the probability of ISC (“heavy atom effect”) in both unimolecular<sup>24</sup> and bimolecular<sup>13,14,25</sup> processes.

ISC between two weakly coupled PESs can also play a central role, as observed for the reaction of the ground state atomic oxygen, O(<sup>3</sup>P), with a variety of molecules in the singlet (ground) electronic state, such as unsaturated (UHs)<sup>15-19</sup> and aromatic hydrocarbons (AHs).<sup>20-22</sup> These reactions proceed mainly via an addition-elimination mechanism and exhibit a significant entrance barrier (up to 20 kJ/mol). The presence of a covalently bound diradical intermediate in the triplet PES makes the jump to the underlying singlet PES more probable. Indeed, ISC occurs in the proximity of such intermediate, which is reached only after the entrance barrier has been overcome.<sup>15-22</sup> In this case, ISC mainly affects

the exit channels and the branching fractions (BFs) of the reaction products. The lifetime of the triplet diradical intermediate determines the extent of ISC, which increases with increasing stability of the diradical.<sup>26,27</sup> Notably, ISC occurs around the initial triplet intermediate also in barrierless reactions, such as C(<sup>3</sup>P)+acetylene.<sup>28,29</sup> Suits and co-workers have reported a more unusual ISC occurring in the exit channel for the bimolecular reaction between O(<sup>3</sup>P) and alkylamines.<sup>30</sup> This kind of outcome is subtle and difficult to clearly discern, as only the reaction mechanism carries the ISC signature while the global rate coefficient is not affected.

In this Article, we report on a hitherto unobserved ISC-based mechanism, thus enlarging the case histories of this important quantum effect. More specifically, we show that ISC can also occur efficiently before the entrance barrier, even in the absence of heavy atoms, as clearly indicated by our experimental results on the reaction between O(<sup>3</sup>P) and pyridine, C<sub>5</sub>H<sub>5</sub>N(X<sup>1</sup>A<sub>1</sub>), one of the simplest aromatic heterocyclic molecules. The study, motivated by the importance of this system in several fields including, e.g., biology, combustion, and astrochemistry,<sup>31-33</sup> led us to propose a new mechanism, in which ISC occurs between two weakly coupled PESs *before* the entrance barrier, following weak interaction of O(<sup>3</sup>P) with the N atom (*ipso* site) of pyridine. This has important consequences on both the reaction rate coefficient and the opening of spin-forbidden reaction channels, such as the mechanism leading to formation of pyrrole and CO, which has been found to be largely dominant in the crossed molecular beam (CMB) experiment here reported. The CMB measurements have been supported by theoretical work featuring quantum-chemical (QC) electronic structure calculations<sup>34</sup> of the triplet and singlet PESs and related RRKM/ME (Rice-Ramsperger-Kassel-Marcus/Master Equation) simulations of product BFs, including ISC, for *meta* and *ipso* addition, as well as nonadiabatic transition state theory (NATST)<sup>35</sup> to determine rate coefficients for ISC reactions.

The synergism between theory and experiment provides unequivocal proof of the mechanism proposed: ISC occurring between two weakly coupled states in the entrance channel, before the entrance

barrier of the triplet PES following a weak interaction of O(<sup>3</sup>P) with the N atom, plays a dominant role in the O(<sup>3</sup>P)+pyridine reaction. Overall, our findings fully support the strong prevalence of the spin-forbidden channel experimentally observed and correctly predict experimental global rate constants. Interestingly, this type of ISC might play a significant role in other reactions between oxygen and nitrogen-containing compounds or, more generally, for bimolecular reactions where a pre-reactive complex is coupled to electronic surfaces of different spin multiplicity before the entrance energy barrier.

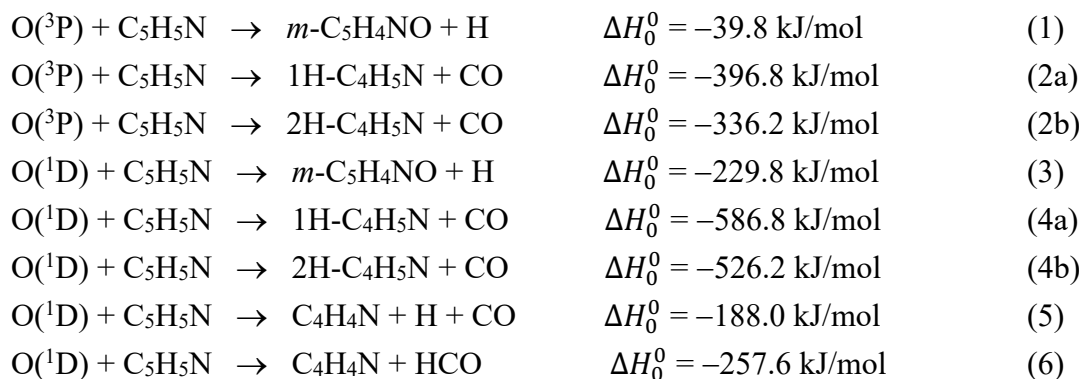
## Results and Discussion

Based on the successful interplay of experiment and theory for the kinetic and dynamic characterization of the O(<sup>3</sup>P)+benzene reaction,<sup>20,22</sup> we have studied the oxidation of pyridine using the same experimental approach combined with accurate QC methodologies to investigate the singlet and triplet reactive PESs. The experimental study was performed under single-collision conditions using the CMB technique with mass-spectrometric (MS) detection and time-of-flight (TOF) analysis (see Methods and Supplementary Information (SI)). Owing to the presence of some ( $\leq 10\%$ ) excited O(<sup>1</sup>D) atoms in the atomic oxygen beam, the dynamics of the pyridine reaction with both O(<sup>3</sup>P) and O(<sup>1</sup>D) was derived (see SI). Exploiting our experience, the energetic characterization of the stationary points of the PESs has been performed using the ‘junChS’ composite scheme<sup>36</sup> (see Methods and SI), on top of structures evaluated with the double-hybrid B2PLYP-D3<sup>37,38</sup> density functional. For key stationary points with a strong multireference character as well as to obtain the structures and energies of the minimum energy crossing points (MECPs) between the singlet and the triplet PESs,<sup>39</sup> CASPT2 calculations with large active spaces<sup>20,22,40</sup> have been exploited (see Methods and SI).

QC calculations of the triplet and singlet PESs point to a variety of energetically-allowed reaction channels for O(<sup>3</sup>P)+pyridine, leading to *o*-, *m*-, *p*-pyridoxyl+H, 1H- and 2H-pyrrole(C<sub>4</sub>H<sub>5</sub>N) CO, open-chain C<sub>4</sub>H<sub>5</sub>N isomers+CO, C<sub>4</sub>H<sub>4</sub>N+HCO, and pyridinyl+OH (see SI). Simplified energy diagrams are sketched in Fig. 1 with the aim of illustrating the main features of the triplet and singlet PESs for the

addition of O(<sup>3</sup>P) to pyridine. It is expected that O(<sup>3</sup>P) adds to the carbon atoms of the heterocyclic aromatic ring predominantly at the *meta* position (Fig. 1a), this being the most activated site for electrophilic attack. Such an expectation is supported by theory that predicts the lowest entrance barrier for *meta* O-addition, followed by the *ortho* and *para* positions (see SI). However, the O(<sup>3</sup>P) electrophilic attack can also occur at the N atom of pyridine (*ipso* addition; Fig. 1b).

Experiment and theory agree in predicting that, due to high barriers (entrance, or exit, or interconversion between isomeric intermediates, see Fig. 1), the only channels relevant at the experimental collision energy ( $E_c = 37.2$  kJ/mol) for both O(<sup>3</sup>P) and O(<sup>1</sup>D) are the following:



While the *m*-pyridoxyl(C<sub>5</sub>H<sub>4</sub>NO)+H products can be obtained from either the triplet (channel (1)) or the singlet (channel (3)) PES, the pyrrole+CO products can be formed from O(<sup>3</sup>P) only via ISC from the entrance triplet PES to the singlet PES (channels (2a,b)) or from O(<sup>1</sup>D) (channels (4a,b)). In addition, particularly relevant to O(<sup>1</sup>D) are also channel (5), the so called “3-body channel”, generated by the fast unimolecular decay of internally hot pyrrole before reaching the detector, and channel (6), leading to pyrrolyl+HCO.

**Experimental results.** In CMB experiments, we have observed all six reaction channels listed previously, and found that, for the O(<sup>3</sup>P) reaction, channels (2) are dominant over channel (1). From laboratory (LAB) product angular and TOF distribution measurements at  $m/z=94$ , 67, and 66, we have characterized the occurrence of the H displacement channels (1) and (3), from data at  $m/z=67$  the pyrrole formation channels (2a,b) and (4a,b), and from data at  $m/z=66$  the 3-body (5) and HCO (6) channels. We

use here the data at  $m/z=66$  and  $67$  to demonstrate the dynamics of the six reaction channels. The angular distributions,  $N(\Theta)$ , and exemplary TOF distributions,  $N(\Theta,t)$ , for  $m/z=66$  and  $m/z=67$  are shown in Fig. 2, together with the velocity vector (Newton) diagram of the experiment (for the complete data set, see SI). In addition to  $m/z=94$ ,  $C_5H_4NO$  (pyridoxyl) products could also be detected (more readily) at  $m/z=66$  (and also at  $m/z=67$ ; see SI) originating from strong dissociative ionization of the parent ion  $C_5H_4NO^+$  in the electron bombardment ionizer. The  $N(\Theta)$ s of  $m/z=66$  and  $67$  exhibit a pronounced, slightly backward-biased distribution with respect to the O atom direction, centred around the CM angle (Figs. 2a and 2c, respectively). The  $N(\Theta)$  of the  $C_5H_4NO$  products at  $m/z=94$  (see SI) and their partial contributions at  $m/z=66$  and  $67$  (Figs. 2a and 2c) are confined to a narrow LAB angular range because of linear momentum conservation, as the H co-product is very light. However, in contrast to  $m/z=94$  (see SI), at both  $m/z=66$  and  $67$  a strong reactive signal is also present at LAB angles well outside the range where the heavy co-products of H channels (1) and (3) are confined, thus suggesting the presence of at least another channel. The different channels can be identified in the TOF spectra  $N(\Theta,t)$  that, although being essentially bimodal (see Figs. 2b and 2d), carry the fingerprint of all six channels (1)-(6).

In Fig. 2, the solid curves superimposed on the experimental results are the calculated curves obtained using the best-fit CM  $T(\theta)$  and  $P(E'_T)$  functions reported in Fig. 3 for the six channels (see Methods and SI). The procedure adopted to determine reaction yields can be summarized as follows. First, experimental data were fitted to determine best-fit CM functions for all the reactions of  $O(^3P)$  and  $O(^1D)$ , starting from the best-fit functions of the related  $O(^3P,^1D)$ +benzene system.<sup>22</sup> The yields for the  $O(^3P)$  and  $O(^1D)$  reactions and their ratio were then computed by summing up all  $O(^3P)$  and  $O(^1D)$  contributions. The quality of the fits, reported in Fig. 2, is demonstrated by the reduced error bars of the best-fit CM distributions for the  $O(^3P)$  and  $O(^1D)$  channels (see Fig. 3), which translate into the uncertainties affecting the BFs of these reaction channels (see Supplementary Table 1).



The  $T(\theta)$  and  $P(E'_T)$  distributions allow an unbiased interpretation of the system dynamics. The  $T(\theta)$  of  $m\text{-C}_5\text{H}_4\text{NO}$  from  $\text{O}(^3\text{P})+\text{pyridine}$ , reported in Fig. 3a (top panel), is distributed over the entire CM angular range and exhibits a clear *backward* peaking ( $\theta=180^\circ$ ). This indicates a direct formation mechanism of  $m\text{-pyridoxyl}+\text{H}$  (channel (1)) on the triplet PES, whereby reactive scattering mainly comes from small impact parameter collisions, which are those determining the preferential *backward* scattering. The relatively low stability of the *meta*-hydroxypyridine diradical in the triplet state,  $^3\text{MIN4}$  at  $-49.5$  kJ/mol with respect to reactants (Fig. 1a), gives further support to this interpretation. The best-fit  $P(E'_T)$  of the  $m\text{-C}_5\text{H}_4\text{NO}+\text{H}$  channel (1) from  $\text{O}(^3\text{P})$ , shown in Fig. 3b (top panel), extends up to about  $77\pm 10$  kJ/mol and is consistent, within the experimental uncertainty, with the calculated total available energy ( $E_{TOT} = E_C - \Delta H_0^0$ ) of  $77.0\pm 5.0$  kJ/mol.

In contrast, the  $T(\theta)$  of pyrrole from  $\text{O}(^3\text{P})+\text{pyridine}$  (Fig. 3a, second panel from top) is isotropic, suggesting that channels (2) proceed via an indirect long-lived complex mechanism<sup>26</sup> on the singlet PES, reached mainly via ISC at  $\text{MECP}_i$  and eventually leading to pyrrole+CO products (see Fig. 1b). The  $P(E'_T)$  of the  $\text{C}_4\text{H}_5\text{N}+\text{CO}$  products reflects a small energy fraction in product translation ( $\langle f_T \rangle = 0.12$ ), indicating that the two molecular co-products are highly internally excited ( $\langle f_{int} \rangle = 0.88$ ), with partial pyrrole fragmentation ( $\approx 10\%$ ) to  $m/z=66$  upon electron ionization. For the reaction dynamics of channel (4) from  $\text{O}(^1\text{D})$  as well as for the dynamics of channels (5) and (6) from  $\text{O}(^1\text{D})$ , the reader is referred to the SI.

The experimentally derived BF<sub>s</sub> for the  $\text{O}(^3\text{P})+\text{pyridine}$  reaction point to a very strong preference ( $\text{BF} = 0.98_{-0.02}^{+0.01}$ ) for the spin-forbidden pyrrole+CO channels (2a,b; experimentally thr 1H- and 2H-pyrrole tautomers cannot be distinguished), while the contribution of the *meta*-pyridoxyl+H channel (1) is marginal ( $\text{BF} = 0.02_{-0.01}^{+0.02}$ ) (see Supplementary Tables 1 and 5, SI). Note that  $\text{BF}=0.16$  for channels (4a,b) and  $\text{BF}=0.014$  for channel (3), while  $\text{BF}=0.78$  for the 3-body channel (5) and  $\text{BF}=0.04$  for the HCO channel (6) (see Supplementary Table 1, SI). Interestingly, the results for the  $\text{O}(^3\text{P})+\text{pyridine}$

reaction are quite different from those found for the  $O(^3P)$  reaction with isoelectronic benzene at comparable  $E_c$ , where the BF for  $C_5H_6(\text{cyclopentadiene})+CO$  is  $0.32\pm 0.16$  (via ISC), while that for the  $H+\text{phenoxy}(C_6H_5O)$  channel is 0.66 (with  $0.48\pm 0.14$  from H loss on the triplet PES and  $0.18\pm 0.06$  on the singlet PES via ISC).<sup>22</sup> The difference between the experimental results for the oxidation of pyridine and benzene by  $O(^3P)$  is therefore remarkable: the spin-forbidden reaction pathways (2) are dominant for pyridine, indeed showing the relevance of ISC in nitrogen-containing AHs, whereas it plays a minor role for  $O(^3P)+\text{benzene}$ .

**Quantum-chemical results.** The energy barrier for H loss and the ISC energy on the triplet PES calculated for the  $O(^3P)$  *meta* addition to pyridine are 57.8 kJ/mol and 27.8 kJ/mol (from <sup>3</sup>MIN4, Fig. 1a), respectively. While the barrier for H loss is only slightly higher than that found in the reaction with benzene (54.4 kJ/mol), the ISC energy is significantly higher (20.9 kJ/mol for benzene<sup>20,22</sup>). In addition, the Landau-Zener parameter determining the probability for triplet to singlet ISC (see SI), namely the ratio between the square of the spin-orbit coupling and the difference in energy gradients between the two PESs at the MECP, was determined using NATST and found to be  $0.30\text{ cm}^{-0.5}$  for benzene and  $0.27\text{ cm}^{-0.5}$  for pyridine. Since the extent of H loss from the triplet PES is the outcome of the competition between ISC and H  $\beta$ -scission, these results indicate that pyridine should favor H loss with respect to benzene on the triplet PES or, if we allow for some uncertainty in the QC calculations, the behavior of the two aromatic compounds should be similar. This is in strong quantitative and qualitative contrast with the experimental evidence, thus suggesting that a different mechanism is at work. Indeed, another pathway exists which leads to efficient ISC and then to pyrrole+CO products. The formation of open-chain isomers of pyrrole was also investigated using the same computational approach as previously described, then followed by ME simulations (see section S2.2.6 of the SI). The overall conclusion is that the pathways leading to the formation of pyrrole are by far the fastest ones.

The main difference between benzene and pyridine is the presence of the tertiary nitrogen atom, with the consequence that H loss is kinetically less favourable than *ipso* addition of O(<sup>3</sup>P). This latter pathway is indeed not competitive with *meta* addition because of the large energy barrier (with respect to reactants): 37.3 kJ/mol (*ipso*) vs 16.5 kJ/mol (*meta*) at the CASPT2 level (see Fig. 1). Alternatively, O(<sup>3</sup>P) can react with the N site of pyridine before the energy barrier and cross directly to the singlet PES. The computed (CASPT2) MECP<sub>i</sub> energy for O(<sup>3</sup>P) *ipso* addition, 8.0 kJ/mol, is quite smaller than that necessary for *ortho*, *meta*, or *para* O(<sup>3</sup>P) addition to pyridine (≥16.5 kJ/mol), thus suggesting that this reaction channel, though spin-forbidden, may compete with *meta* addition (Fig. 1). As a matter of fact, the computed BFs for the *ipso* attack are 0.96 for CO formation and 0.04 for H elimination, both via ISC on the singlet surface, while the corresponding results for the *meta* attack are 0.70 and 0.01, but, in this case, a non-negligible amount of H (0.29) is obtained from the triplet surface (see Supplementary Table 5, SI, for further details). The nice agreement of the *ipso* results with the experimental results (BF of 0.98<sup>+0.01</sup><sub>-0.02</sub> for CO formation) gives further support to the proposed mechanism. The computed PES shows that two main tautomers of pyrrole can be formed, 1H-pyrrole and 2H-pyrrole (see Fig. 1). Although their relative yield cannot be obtained from the experiment, the statistical calculations indicate that the less exothermic 2H-pyrrole+CO channel is favoured with respect to the more exothermic 1H-pyrrole+CO counterpart by a factor of 2.4. This indicates that ISC is very efficient in the O(<sup>3</sup>P)+pyridine reaction at E<sub>c</sub>=37.2 kJ/mol. Furthermore, ISC leading to pyrrole+CO can occur not only in the region of the covalently bound diradical complex (located past the entrance barrier (<sup>3</sup>TS2) of 16.5 kJ/mol), following *meta* addition, in a mechanism similar to O(<sup>3</sup>P)+benzene, but also by ISC in the entrance channel of the PES, before the high (37.3 kJ/mol) entrance barrier (<sup>3</sup>TS15) following *ipso* attack. Though the pre-reactive complex found in this channel has a short lifetime and was therefore not included explicitly in the ME simulations, the long-range interaction established on the triplet electronic PES between O(<sup>3</sup>P) and the nitrogen lone pair (a three electron - two orbital system) has a direct impact on the energy of the

MECP<sub>i</sub>, and thus on the rate of this channel with respect to that of competitive entrance channels. Indeed, extensive computational investigations were unable to find any pre-reactive complex in the entrance channels of the O(<sup>3</sup>P) addition at *ortho*, *meta*, and *para* positions.

**Kinetic calculations.** Fig. 4 shows the comparison between the experimental and computed rate constants for O(<sup>3</sup>P)+pyridine as a function of temperature (T). For calculated rate constants, the ISC pathway via *ipso* addition, the pathway via *meta* addition, and the direct H abstraction pathway (in the most favourable *ortho* position, leading to OH formation) are distinguished. It is apparent that the ISC rate from *ipso* addition is prevalent at low T, while the rate of *meta* addition becomes equal to that of ISC via *ipso* addition at T ≈ 400 K, and tends to prevail at higher T. The contribution of H *ortho* abstraction becomes significant only at very high T (>900 K) because of a high energy barrier (39.6 kJ/mol) and overall endothermicity (20.5 kJ/mol, see Fig. 1a). The change of mechanism going from high to low temperatures is accompanied by a significant change in activation energy, which varies from 26.2 kJ/mol, as derived by Frerichs et al.<sup>41</sup> in the 370-670 K temperature range, to 10.5 kJ/mol, as determined by Tabares et al.<sup>42</sup> in the 323-473 K temperature range. This trend is consistent with the non-Arrhenius behavior usually observed in reactions where quantum effects are important.<sup>4,7</sup> Most notably, once the system is on the singlet PES following *ipso* addition and ISC, the most favourable product channel is that leading, after several interconversions, to pyrrole+CO (channels (2a,b); see Fig. 1b), which corroborates the very high branching fraction (BF=0.98) of these spin-forbidden channels (2) found in the CMB experiments.

**A frontier orbital interpretation.** From a qualitative point of view, the difference between *ipso* and *meta* O(<sup>3</sup>P) attacks can be explained considering that, for this 50-electron system, the three low-lying electronic states ruling ISC can be obtained from different distributions of the four valence electrons of the oxygen atom in the orbitals 24, 25, and 26 shown in Fig. 5. These electronic configurations are (2,2,0) for the lowest singlet state (S<sub>0</sub>), and (2,1,1) or (1,2,1) for the two lowest triplet states (T<sub>1</sub> and T<sub>2</sub>,

respectively) involved in ISC. The frontier orbitals of MECP<sub>m</sub> (Fig. 5b) and for the MECP of the benzene+O(<sup>3</sup>P) system (Fig. 5c) are similar, thus leading to comparable spin-orbit couplings.<sup>20,22</sup> However, as can be seen from Fig. 5, the orbitals of the MECP<sub>i</sub> (Fig. 5a) have a different nature and, in particular, orbital 26, which is singly occupied in the T<sub>1</sub> and T<sub>2</sub> states, involves a strong  $\sigma$  antibonding interaction between oxygen and nitrogen. This effect is conceivably non-negligible already at long O–N distances, i.e., before the entrance barrier of the *ipso* approach, near the pre-reactive complex (for a more detailed analysis of the orbitals, see SI). Furthermore, in the entrance channel the angular momentum of the frontier orbitals changes between triplet and singlet states, a feature diagnostic of strong spin-orbit coupling according to the El-Sayed rules.<sup>43</sup> Noted is that an analogous situation was found by Li et al. in the case of ISC in the exit channel.<sup>30</sup>

**Energy specificity in promoting reactivity.** The energy barrier governing the *meta* addition is essentially determined by the strain energy required by the out-of-plane deformation of the pyridine ring (about 15 kJ/mol) and, in the associated TS, the structure of pyridine is significantly distorted with respect to the reactant structure. In kinetic experiments at room T or above, excited low-frequency out-of-plane vibrations of pyridine have non-negligible Boltzmann populations and can be very efficient in promoting reactivity. In CMB experiments, because of the cooling associated with supersonic expansion, those low-frequency vibrational modes are in their ground level and all the energy available to the system comes from the reactant translational energy. But this is a form of energy which is not suitable to promote internal deformations due to the lack of efficient couplings. On the other hand, the structure of the MECP governing the *ipso* addition involves a negligible deformation of the pyridine ring (about 3 kJ/mol), thus resembling an early-TS. In other words, we can consider the TS associated with the *meta* approach as a late-TS, for which the most efficient form of energy to promote reactivity is the vibrational excitation of the molecular reactant, and that associated with the *ipso* approach as an early-TS, for which the most efficient form of energy is translational energy of the reactants. Therefore, the apparent inconsistency

between kinetics and CMB experiments can be resolved by considering the energy specificity in promoting reactivity, as described by the Polanyi rules (see SI, section 2.2.6, for deeper details and references).

## Conclusions and outlook

CMB measurements show that the dominant (BF=0.98) reaction channel of O(<sup>3</sup>P)+pyridine is the spin-forbidden pathway leading to pyrrole+CO, with the *meta*-pyridoxyl+H channel playing only a marginal role (BF = 0.02<sup>+0.02</sup><sub>-0.01</sub>). The experimentally estimated extent of ISC is then about 98%, in sharp contrast to what was observed for the reaction of O(<sup>3</sup>P) with the isoelectronic benzene molecule,<sup>22</sup> where H production is ruled by the spin-allowed triplet pathway with BF=0.66 (0.48 from triplet PES and 0.18 from singlet PES via ISC). Interestingly, theory suggests that ISC to the singlet PES, leading to formation of 1H- and 2H-pyrrole+CO (in a 1/2.4 ratio) occurs in the entrance channel before the barrier, following the *ipso* interaction between the O atom and the lone pair of the N atom of pyridine on the triplet PES. To the best of our knowledge, the detection of ISC in the entrance channel in the absence of heavy atoms (e.g., iodine) has never been reported previously. Remarkably, the computed ISC rate before the entrance barrier determines the overall reaction rate at low and moderate temperatures, in agreement with the kinetic results. When active, this newly found reaction mechanism is expected to contribute to the system reactivity near or below room temperature at any pressure.

Our combined experimental and theoretical investigation provides evidence that the O(<sup>3</sup>P)+pyridine reaction mechanism involving ISC before the entrance barrier may play a role in bimolecular reactions with the same characteristics. Given that important biomolecules, including nucleobases, are N-heterocyclic aromatic compounds, the quite unexpected outcome of the present study devoted to the reaction of pyridine with atomic oxygen may have implications in biological processes. Finally, the present results suggest a possible destruction pathway of pyridine hitherto unobserved in different environments such as the interstellar medium.

## **Acknowledgements**

This work has been supported by the Italian MUR (PRIN 2017 - Grant 2017A4XRCA (VB); PRIN 2017 - Grant 2017PJ5XXX (PC); PRIN 2020 – Grant 202082CE3T (CP)) and the Italian Space Agency (ASI; ‘Life in Space’ project, N. 2019-3-U.0 (NB,VB)). The authors acknowledge the Scuola Normale Superiore (Internal Funds), the University of Bologna (RFO funds), the Italian MUR and Università degli Studi di Perugia (within the program “Department of Excellence–2018–2022–Project AMIS”), and the SMART@SNS Laboratory (<http://smart.sns.it>) for high-performance computer facilities.

## **Authors contributions**

G. V., G. P., P. R., D. M., A. C., and V. J. M. performed the experiments and analyzed the data; S. A. and A. B. performed the quantum-chemical computations and analyzed the results; P. C. and N. B. conceived and guided the experiments and the interpretation of its results; C. C., C. P. and V. B conceived the computational strategy and coordinated the interpretation of its results; P. C., N. B., C. C., C. P. and V. B. co-wrote the paper. All authors discussed the results and commented on the manuscript.

## **Competing interests**

The authors declare no competing interests.

## Figure Captions

**Fig. 1 | Schematic, simplified representation of the triplet (red lines) and singlet (blue lines) PESs of the O+pyridine reaction for O(<sup>3</sup>P) *meta* and *ipso* addition.** **a**, Addition of O(<sup>3</sup>P) on the C atom in *meta* position, and direct H abstraction. **b**, *Ipso* addition of O(<sup>3</sup>P) on the lone pair of the N atom of pyridine. The location of the minimum energy crossing point (MECP) between the entrance triplet PES and the singlet PES following *meta* (**a**) and *ipso* (**b**) attack, where an ISC occurs, is indicated with a circle. Continuous lines are used for the main observed channels (red for triplet and blue for singlet pathways), while dashed lines indicate pathways to product channels which are negligible under the present experimental conditions. Relative energies (in kJ/mol) are at the junChS level of theory (except for MECPS, which are at the CAPT2 level) and incorporate the zero-point energy correction.

**Fig. 2 | Product laboratory (LAB) angular and time-of-flight (TOF) distributions.** **a, c**, Product LAB angular distribution,  $N(\Theta)$ , at  $m/z=66$  and  $m/z=67$ , respectively, for the  $O(^3P, ^1D)+C_5H_5N$  reactions at  $E_c=37.2$  kJ/mol. Data (solid dots) are presented as mean value  $\pm 1$  SD of five angular scans. **b, d**, Product TOF distributions,  $N(\Theta, t)$ , at five selected LAB angles for  $m/z = 66$  and  $m/z=67$ , respectively. In panels **a-d** the solid black curve is the total distribution calculated with the best-fit CM functions (shown in Fig. 3) for the six contributing reactive channels; the latter are color-coded and specified. The complete TOF data set is provided in the SI. **e**, Velocity vector (so-called Newton) diagram of the experiment. Circles (colour-coded as in **a-d**) delimit the angular distribution range of products from O(<sup>3</sup>P) and O(<sup>1</sup>D) in the LAB frame. The circle radius indicates the maximum velocity that the corresponding indicated product (the co-product is given in parenthesis) can attain in the CM frame by assuming that all the available energy (given by  $E_c-\Delta H^0$ ) is channelled into product translational energy.

**Fig. 3 | Best-fit centre-of-mass (CM) product angular and translational energy distributions.** Best-fit CM angular distributions  $T(\theta)$  (**a**) and translational energy distributions  $P(E_T')$  (**b**) determined for the reactive channels of  $C_5H_4NO+H$  (red) and  $C_4H_5N+CO$  (blue) from the reaction of O(<sup>3</sup>P)+pyridine, and  $C_5H_4NO+H$  (orange),  $C_4H_5N+CO$  (green),  $C_4H_4N+H+CO$  (magenta), and  $C_4H_4N+HCO$  (violet) from the reaction of O(<sup>1</sup>D)+pyridine. The total energy,  $E_{TOT}$  ( $E_{TOT}=E_c-\Delta H^0$ ), and the translational energy fraction,  $\langle f_T \rangle$ , determined for each reactive channel are also reported. The shaded areas represent the error bars (upper and lower bounds) determined for the CM functions. Upper and lower bounds delimit CM functions that still afford an acceptable fit of the LAB data.

**Fig. 4 | Total and single-channel rate constants.** The total and channel-specific rate constants computed for the O(<sup>3</sup>P)+pyridine reaction using conventional and nonadiabatic transition state theory, compared with experimental data (mean value  $\pm 1$  SD) for the total rate constant from Frerichs et al.<sup>41</sup> and Tabares et al.<sup>42</sup> as reported and rescaled for the ratio between the O(<sup>3</sup>P)+benzene rate constant measured by the same authors and that recently computed for the same reaction. The detailed explanation is provided in the SI.

**Fig. 5 | Frontier Orbitals of the relevant Minimum Energy Crossing Points.** Frontier orbitals for MECPS (**a**), MECPS<sub>*m*</sub> (**b**) and benzene MECPS (**c**) obtained from  $\omega$ B97X-D/6-311+G(d,p) computations and plotted with isodensity surfaces at  $\pm 0.03$  e Bohr<sup>3</sup>. The occupations of orbitals 24, 25 and 26 are (2,2,0), (2,1,1) and (1,2,1) for the S<sub>0</sub>, T<sub>1</sub>, and T<sub>2</sub> electronic state, respectively. The strong difference of orbital 26 for the *ipso* attack on pyridine (a strong  $\sigma$  antibonding interaction) with respect to MECPS<sub>*m*</sub> and benzene MECPS plays a key role in explaining its peculiar long-range ISC.



## References

- 1 Bao, J. L. & Truhlar, D. G. Variational transition state theory: theoretical framework and recent developments. *Chem. Soc. Rev.* **46**, 7548-7596 (2017).
- 2 Smith, I. W. M. The temperature-dependence of elementary reaction rates: beyond Arrhenius. *Chem. Soc. Rev.* **37**, 812-826 (2008).
- 3 Smith, I. W. M. Laboratory Astrochemistry: Gas-Phase Processes. *Annu. Rev. Astron. Astrophys.* **49**, 29-66 (2011).
- 4 Sims, I. R. Tunnelling in space. *Nat Chem* **5**, 734-736 (2013).
- 5 Tizniti, M. *et al.* The rate of the F + H<sub>2</sub> reaction at very low temperatures. *Nat Chem* **6**, 141-145 (2014).
- 6 Shannon, R. J., Blitz, M. A., Goddard, A. & Heard, D. E. Accelerated chemistry in the reaction between the hydroxyl radical and methanol at interstellar temperatures facilitated by tunnelling. *Nat Chem* **5**, 745-749 (2013).
- 7 Heard, D. E. Rapid Acceleration of Hydrogen Atom Abstraction Reactions of OH at Very Low Temperatures through Weakly Bound Complexes and Tunneling. *Acc. Chem. Res.* **51**, 2620-2627 (2018).
- 8 Harvey, J. N. Understanding the kinetics of spin-forbidden chemical reactions. *Phys. Chem. Chem. Phys.* **9**, 331-343 (2007).
- 9 Ahmadvand, S., Zaari, R. R. & Varganov, S. A. Spin forbidden and spin-allowed cyclopropanone (*c*-H<sub>2</sub>C<sub>3</sub>O) formation in interstellar medium. *Astrophys. J.* **795**, 173 (2014).
- 10 Jasper, A. W. Multidimensional Effects in Nonadiabatic Statistical Theories of Spin-Forbidden Kinetics: A Case Study of <sup>3</sup>O + CO → CO<sub>2</sub>. *J. Phys. Chem. A* **119**, 7339-7351 (2015).
- 11 Domcke, W., Yarkony, D. & Köppel, H. *Conical intersections: electronic structure, dynamics & spectroscopy*. Vol. 15 (World Scientific, Singapore 2004).
- 12 Shen, L. *et al.* Role of Multistate Intersections in Photochemistry. *J. Phys. Chem. Lett.* **11**, 8490-8501, doi:10.1021/acs.jpcclett.0c01637 (2020).
- 13 Wang, J. J., Smith, D. J. & Grice, R. Role of Intersystem Crossing in the Dynamics of the O(<sup>3</sup>P) + (CH<sub>3</sub>)<sub>2</sub>CHI, (CH<sub>3</sub>)<sub>3</sub>CI Reactions. *J. Phys. Chem.* **100**, 13603-13608 (1996).
- 14 Stevens, J. E., Cui, Q. & Morokuma, K. An *ab initio* investigation of spin-allowed and spin-forbidden pathways of the gas phase reactions of O(<sup>3</sup>P)+C<sub>2</sub>H<sub>5</sub>I. *J. Chem. Phys.* **108**, 1544-1551 (1998).
- 15 Fu, B. *et al.* Intersystem crossing and dynamics in O(<sup>3</sup>P) + C<sub>2</sub>H<sub>4</sub> multichannel reaction: Experiment validates theory. *Proc. Natl. Acad. Sci. U.S.A* **109**, 9733-9738 (2012).
- 16 Gimondi, I., Cavallotti, C., Vanuzzo, G., Balucani, N. & Casavecchia, P. Reaction Dynamics of O(<sup>3</sup>P) + Propyne: II. Primary Products, Branching Ratios, and Role of Intersystem Crossing from Ab Initio Coupled Triplet/Singlet Potential Energy Surfaces and Statistical Calculations. *J. Phys. Chem. A* **120**, 4619-4633 (2016).
- 17 Leonori, F. *et al.* Experimental and Theoretical Studies on the Dynamics of the O(<sup>3</sup>P) + Propene Reaction: Primary Products, Branching Ratios, and Role of Intersystem Crossing. *J. Phys. Chem. C* **119**, 14632-14652 (2015).
- 18 Leonori, F. *et al.* Crossed Molecular Beam Dynamics Studies of the O(<sup>3</sup>P) + Allene Reaction: Primary Products, Branching Ratios, and Dominant Role of Intersystem Crossing. *J. Phys. Chem. Lett.* **3**, 75-80 (2012).
- 19 Savee, J. D. *et al.* Multiplexed Photoionization Mass Spectrometry Investigation of the O(<sup>3</sup>P) + Propyne Reaction. *J. Phys. Chem. A* **119**, 7388-7403 (2015).
- 20 Cavallotti, C. *et al.* Theoretical Study of the Extent of Intersystem Crossing in the O(<sup>3</sup>P) + C<sub>6</sub>H<sub>6</sub> Reaction with Experimental Validation. *J. Phys. Chem. Lett.* **11**, 9621-9628 (2020).
- 21 Taatjes, C. A. *et al.* Products of the Benzene + O(<sup>3</sup>P) Reaction. *J. Phys. Chem. A* **114**, 3355-3370 (2010).
- 22 Vanuzzo, G. *et al.* Crossed-Beam and Theoretical Studies of the O(<sup>3</sup>P, <sup>1</sup>D) + Benzene Reactions: Primary Products, Branching Fractions, and Role of Intersystem Crossing. *J. Phys. Chem. A* **125**, 8434-8453 (2021).
- 23 He, C. *et al.* Non-Adiabatic Reaction Dynamics in the Gas-Phase Formation of Phosphinidenesilylene, the Isovalent Counterpart of Hydrogen Isocyanide, under Single-Collision Conditions. *J. Phys. Chem. Lett.* **12**, 2489-2495 (2021).
- 24 Koziar, J. C. & Cowan, D. O. Photochemical heavy-atom effects. *Acc. Chem. Res.* **11**, 334-341 (1978).
- 25 Alagia, M. *et al.* Crossed Beam Studies of the O(<sup>3</sup>P, <sup>1</sup>D)+CH<sub>3</sub>I Reactions: Direct Evidence of Intersystem Crossing for Bent Geometries. *Faraday Discuss.* **113**, 133-150 (1999).
- 26 Pan, H., Liu, K., Caracciolo, A. & Casavecchia, P. Crossed beam polyatomic reaction dynamics: recent advances and new insights. *Chem. Soc. Rev.* **46**, 7517-7547 (2017).
- 27 Casavecchia, P., Leonori, F. & Balucani, N. Reaction dynamics of oxygen atoms with unsaturated hydrocarbons from crossed molecular beam studies: primary products, branching ratios and role of intersystem crossing. *Int. Rev. Phys. Chem.* **34**, 161-204 (2015).
- 28 Mebel, A. M., Kislov, V. V. & Hayashi, M. Prediction of product branching ratios in the C(<sup>3</sup>P)+C<sub>2</sub>H<sub>2</sub>→*l*-C<sub>3</sub>H+H/*c*-C<sub>3</sub>H+HC<sub>3</sub>+H<sub>2</sub> reaction using ab initio coupled clusters calculations extrapolated to the complete basis set combined with Rice-Ramsperger-Kassel-Marcus and radiationless transition theories. *J. Chem. Phys.* **126**, 204310 (2007).

- 29 Leonori, F. *et al.* Unraveling the Dynamics of the  $C(^3P,^1D) + C_2H_2$  Reactions by the Crossed Molecular Beam Scattering Technique. *J. Phys. Chem. A* **112**, 1363-1379 (2008).
- 30 Li, H., Kamasah, A., Matsika, S. & Suits, A. G. Intersystem crossing in the exit channel. *Nat Chem* **11**, 123-128 (2019).
- 31 Wang, B. *et al.* A kinetic study of NO formation during oxy-fuel combustion of pyridine. *Appl. Energy* **92**, 361-368 (2012).
- 32 Parker, D. S. N. *et al.* On the formation of pyridine in the interstellar medium. *Phys. Chem. Chem. Phys.* **17**, 32000-32008 (2015).
- 33 Puzzarini, C. & Barone, V. A never-ending story in the sky: The secrets of chemical evolution. *Phys. Life Rev.* **32**, 59-94 (2020).
- 34 Puzzarini, C., Bloino, J., Tassinato, N. & Barone, V. Accuracy and Interpretability: The Devil and the Holy Grail. New Routes across Old Boundaries in Computational Spectroscopy. *Chem. Rev.* **119**, 8131-8191 (2019).
- 35 Klippenstein, S. J. & Cavallotti, C. in *Computer Aided Chemical Engineering* Vol. 45 (eds Tiziano Faravelli, Flavio Manenti, & Eliseo Ranzi) 115-167 (Elsevier, 2019).
- 36 Alessandrini, S., Barone, V. & Puzzarini, C. Extension of the "Cheap" Composite Approach to Noncovalent Interactions: The jun-ChS Scheme. *J. Chem. Theory Comput.* **16**, 988-1006 (2020).
- 37 Grimme, S. Semiempirical hybrid density functional with perturbative second-order correlation. *J. Chem. Phys.* **124**, 034108 (2006).
- 38 Biczysko, M., Panek, P., Scalmani, G., Bloino, J. & Barone, V. Harmonic and Anharmonic Vibrational Frequency Calculations with the Double-Hybrid B2PLYP Method: Analytic Second Derivatives and Benchmark Studies. *J. Chem. Theory Comput.* **6**, 2115-2125 (2010).
- 39 Kaliakin, D. S., Fedorov, D. G., Alexeev, Y. & Varganov, S. A. Locating Minimum Energy Crossings of Different Spin States Using the Fragment Molecular Orbital Method. *J. Chem. Theory Comput.* **15**, 6074-6084 (2019).
- 40 Pulay, P. A perspective on the CASPT2 method. *Int. J. Quantum Chem.* **111**, 3273-3279 (2011).
- 41 Frerichs, H., Schliephake, V., Tappe, M. & Wagner, H. G. Reactions of Pyridine and the Picolines with Atomic Oxygen ( $O^3P$ ) in the Gas Phase. *Zeitsch. Phys. Chem.* **166**, 157-165 (1990).
- 42 Tabares, F. & Gonzalez Urena, A. Rate constant for the reaction of atomic oxygen ( $^3P$ ) with pyridine from 323 to 473 K. *J. Phys. Chem.* **87**, 4933-4936 (1983).
- 43 El-Sayed, M. A. Triplet state. Its radiative and nonradiative properties. *Acc. Chem. Res.* **1**, 8-16 (1968).

## Methods

**Experiment.** The pyridine+O(<sup>3</sup>P,<sup>1</sup>D) reaction dynamics were studied using the CMB technique, coupled with MS detection and TOF analysis. The apparatus and methodology employed are analogous to those of previous works on the dynamics of O(<sup>3</sup>P) reactions with unsaturated hydrocarbons and benzene.<sup>15,16,17,18,20,22,26,27</sup> Continuous supersonic beams of the two reactants are crossed at 90° in a high-vacuum chamber kept at 8×10<sup>-7</sup> mbar by extensive magnetically suspended turbo- and cryo-pumping (base pressure 1×10<sup>-7</sup> mbar). The reaction products are detected by a tunable electron impact ionizer followed by a quadrupole mass filter and a Daly type ion detector, housed in a ultra-high-vacuum chamber (<10<sup>-10</sup> mbar) that can rotate around the scattering centre in the plane of the beams.<sup>20,22,26,27</sup> Pyridine (C<sub>5</sub>H<sub>5</sub>N, 98% purity) was stored inside a stainless-steel container kept at 296 K. Bubbling He gas in the liquid, a He-seeded supersonic beam of pyridine was produced expanding 260 mbar of the gas mixture through a 0.1 mm diameter nozzle (kept at 301 K), followed by a 0.8 mm skimmer and a further defining aperture. The supersonic O atom beam was generated using a radiofrequency discharge beam source<sup>27,44</sup> operating at 300 W, expanding a 5% O<sub>2</sub> in He gas mixture (90 mbar) through a 0.48 mm diameter water-cooled quartz nozzle, followed by a 0.9 mm diameter boron nitride skimmer and a further collimating aperture. The atomic oxygen beam mainly contains ground-state O(<sup>3</sup>P) and a small amount of excited O(<sup>1</sup>D) (≤10%).<sup>44</sup> Under these conditions, the reactant velocities were 973 and 2154 m s<sup>-1</sup>, with a speed ratio of 7.0 and 4.2 for C<sub>5</sub>H<sub>5</sub>N and O atoms, respectively. The resulting collision energy (E<sub>c</sub>) was 37.2 kJ/mol. The oxygen and pyridine beam angular divergence is 2.3° and 3.8°, respectively; the detector angular resolution for a point collision zone is 1.1°.

Product LAB angular distributions, N(Θ), at selected mass-to-charge ratios (*m/z*) were acquired by modulating the C<sub>5</sub>H<sub>5</sub>N beam at 160 Hz for background subtraction. Product time-of-flight (TOF) distributions, N(Θ,t), were measured using the pseudorandom-chopping method at 6 μs/channel. In all measurements, *hard* electron-impact ionization (70 eV) was employed.<sup>27</sup> Reactive scattering signals were observed at mass-to-charge ratios (*m/z*) of 94 (C<sub>5</sub>H<sub>4</sub>NO<sup>+</sup>), 93 (C<sub>5</sub>H<sub>3</sub>NO<sup>+</sup>), 67 (C<sub>4</sub>H<sub>5</sub>N<sup>+</sup>), and 66 (C<sub>4</sub>H<sub>4</sub>N<sup>+</sup>), with relative intensities at the centre of mass (CM) angle of 0.11, 0.06, 0.11, and 1.00, respectively. Product angular distributions were measured at *m/z*= 94, 67, and 66 (see Supplementary Fig. 1). Product TOF distributions were recorded for *m/z*=66 at ten different LAB angles (see Supplementary Fig. 2) and for *m/z*=67 at six different LAB angles (see Supplementary Fig. 3). A selection of these data is reported in Figs. 2a-d.

To derive quantitative information on the reaction dynamics from the raw data, one has to move from the laboratory (LAB) frame to the CM frame, and hence analyse the total CM product flux,  $I_{CM}(\theta, E'_T)_{total}$ .<sup>26,27</sup> This can be conveniently factorized into the angular,  $T(\theta)$ , and translational energy,  $P(E'_T)$ , distributions.<sup>22,26,27</sup> Because of the experimental conditions (finite angular and velocity distribution of the reactants and detector angular resolution), the best-fit CM functions are actually

derived by a forward convolution fit of the total product LAB angular and TOF distributions at a given  $m/z$  value as follows:  $I_{CM}(\theta, E'_T)_{total} = \sum_i w_i \times [T(\theta)_i \times P(E'_T)_i]$ , with the best-fitting parameter  $w_i$  representing the relative contribution of the apparent integral cross section of the  $i^{\text{th}}$  channel.<sup>27</sup> We have determined the product branching fractions (BFs) following a procedure successfully applied in recent studies of several polyatomic multichannel reactions of O(<sup>3</sup>P) with unsaturated hydrocarbons.<sup>16,17,18,20,22,27,29</sup> The parameters considered are: the channel apparent cross sections ( $w_i$ ) derived from the best-fit analysis, the estimated electron ionization cross sections, and the measured total yield of the primary products, also taking into account ion fragmentation and quadrupole transmission.<sup>27</sup> For further details about experimental data, data analysis and overall results, the reader is referred to the SI.

Similarly to what observed in a recent detailed study of the related O(<sup>3</sup>P,<sup>1</sup>D)+benzene reaction,<sup>22</sup> in order to simultaneously fit the LAB angular and TOF distributions at  $m/z=66$  (Figs. 2a and 2b), it was necessary to invoke: (i) two contributions for the signal attributable to C<sub>5</sub>H<sub>4</sub>NO, one coming from the O(<sup>3</sup>P) channel (1) and the other from the O(<sup>1</sup>D) channel (3), which together determine the intense peak near the CM angle in the N( $\Theta$ ) and the slow, intense peak in the N( $\Theta$ ,t) TOF spectra; (ii) a strong contribution attributed to the 3-body channel (5) from O(<sup>1</sup>D), which determines most of the wing intensity in the N( $\Theta$ ) and nearly all of the fast peak in the TOF spectra; (iii) a small contribution attributed to the HCO+pyrrolyl channel (6), necessary to fill-up the deep gap between the fast and slow peaks in the TOF spectra and predict the right shape of the N( $\Theta$ ) around  $\Theta=50^\circ$ ; (iv) two very small contributions of pyrrole from channels (2) and (4), which are not discernable on the figure scale. Analogously, to fit the  $m/z=67$  data (Figs. 2c and 2d) it was necessary to invoke: (i) two contributions for the signal ascribable to C<sub>5</sub>H<sub>4</sub>NO, one coming from the O(<sup>3</sup>P) channel (1) and the other from the O(<sup>1</sup>D) channel (3), analogously to the  $m/z=66$  data; (ii) two contributions from pyrrole, one from the O(<sup>3</sup>P) channels (2), corresponding to the slow part of the fast TOF peak and for the curvature of N( $\Theta$ ) near  $\Theta=40^\circ$ , and the other from the O(<sup>1</sup>D) channels (4), corresponding to the fast side of the fast TOF peak. A detailed data analysis and discussion, and a comparison with the closely related O(<sup>3</sup>P,<sup>1</sup>D)+benzene system, are reported in the SI. The signal of the heavy co-product (pyridoxyl, C<sub>5</sub>H<sub>4</sub>NO) of the H-forming channel, representing only a few percent of the total yield, appears much stronger in the LAB frame than that of a much more abundant product (pyrrole) from a channel of two co-products of comparable mass, such as the pyrrole+CO channel (see, for instance, Figs. 2a-d). The reason is that, because of linear momentum conservation, the heavy co-product of the H channel is distributed within a very narrow Newton sphere in the CM frame (see Fig. 2e), and this leads to a strong enhancement in the LAB frame because of the Jacobian transformation relating the CM and LAB frames (see SI). It is recalled that the average product translational energy  $\langle E'_T \rangle$  is defined as  $\langle E'_T \rangle = \sum P(E'_T)E'_T / \sum P(E'_T)$ , and the average fraction of total available energy,  $E_{TOT} = E_c - \Delta H_0^0$ , channelled into translation,  $\langle f_T \rangle$  (see Fig. 4b), is defined as  $\langle f_T \rangle = \langle E'_T \rangle / E_{TOT}$ .<sup>27</sup>

**Quantum chemistry.** The reaction between pyridine and atomic oxygen has been investigated on both the triplet and singlet PESs. A preliminary investigation of all possible attacks of O(<sup>3</sup>P,<sup>1</sup>D) and their energetic evolution was carried out using the hybrid B3LYP functional in conjunction with a double-zeta quality basis set, also incorporating D3 dispersion corrections.<sup>45,46</sup> The same level of theory was employed to confirm the nature of all stationary points, thus providing the corresponding harmonic zero-point vibrational energies (ZPEs). To ensure the correct connection between transition state (TS) structures and minima, intrinsic reaction coordinate (IRC) analyses were performed at this level of theory throughout the PESs.<sup>47</sup> The most significant stationary points were subsequently re-optimized using the double-hybrid B2PLYP-D3 functional in conjunction with the maug-cc-pVTZ-*d*H basis set.<sup>37,38,45,48</sup> On top of these improved structures, the electronic energy was refined using the junChS composite scheme,<sup>36</sup> which is based on coupled-cluster theory and accounts for extrapolation to the complete basis set limit and for effects due to correlation of inner electrons. The central term is the energy computed using the CC theory with a full account of single and double excitations and a perturbative treatment of triples, CCSD(T),<sup>49</sup> in conjunction with the partially augmented jun-cc-pVTZ basis set.<sup>48</sup> This term is computed within the frozen-core (fc) approximation. Møller-Plesset perturbation theory to the second order<sup>50</sup> (MP2) is then used to recover the basis-set truncation error by extrapolating the fc-MP2 energies to the complete basis set (CBS) limit. This requires computations with two basis sets of the hierarchical jun-cc-pVnZ family (*n*=T and Q). The missing contribution of the correlation of inner electrons is added by computing the energy difference between two MP2 computations, one correlating all electrons and the other one carried out within the fc approximation, both in the same basis set (cc-pwCVTZ).<sup>51</sup>

The final energy barriers reported in Fig. 1 and in the SI were obtained by combining junChS electronic energies with harmonic B3LYP ZPE corrections, and have an estimated accuracy of about 1-5 kJ/mol.<sup>36,52,53</sup> An extensive account on the computational strategy employed is reported in the SI. All these computations were performed using the Gaussian16 quantum-chemistry package.<sup>54</sup> A detailed account of the quantum-chemical calculations is provided in the SI.

MECPs between the triplet and the singlet PES were determined at two levels of theory. First, MECPs following O(<sup>3</sup>P) addition at *ortho*, *meta*, and *para* positions, as well as the MECP for ISC taking place contextually to *ipso* addition were determined at the same level of theory ( $\omega$ B97X-D/6-311+G(d,p))<sup>55,56</sup> used in the previous study of the benzene+O(<sup>3</sup>P) reaction,<sup>20,22</sup> employing the automatic procedure implemented in the EStokTP code.<sup>57</sup> Similarly to benzene, we found a significant SO coupling of about 35 cm<sup>-1</sup> between the T<sub>2</sub> and S<sub>0</sub> states for the *ortho*, *meta*, and *para* MECPs, while in the case of *ipso* addition T<sub>1</sub>/S<sub>0</sub> and T<sub>2</sub>/S<sub>0</sub> have similar SO couplings (40 cm<sup>-1</sup>) and energies. The *ipso* MECP was determined also at the CASPT2 level, using a (12e,10o) active space including the (4e,3o) p orbitals and electrons of O(<sup>3</sup>P), the six  $\pi$  electrons, and bonding and antibonding orbitals of pyridine and the N lone pair. All structures were optimized using the jun-cc-pVTZ

basis set and the corresponding energies were determined accounting for basis-set size and active space increase by inclusion of the four N-C  $\sigma$  and  $\sigma^*$  orbitals, as described in detail in the SI. This level of theory was also employed to refine the energy barriers of the *meta* and *ipso* addition reactions, which have significant multireference character. Rate constants were computed using NATST and conventional TST, as described in the SI. All CASPT2 calculations were performed using the Molpro 2020 program.<sup>58</sup>

**Kinetics.** Rate constants within a single PES and involving non negligible energy barriers were computed using conventional transition state theory (TST) within the Rigid-Rotor Harmonic-Oscillator Approximation, as implemented in the EStokTP code. The rate of ISC taking place contextually to *ipso* addition was computed using non-adiabatic transition state theory (NATST),<sup>59</sup> with transition probabilities determined using Landau-Zener (LZ) theory.<sup>60,61</sup> Rate constants for barrierless reactions were determined using variable reaction coordinate transition state theory (VRC-TST) with the VaReCoF code,<sup>62</sup> recently interfaced with EStokTP. Further details are given in the SI.

Master Equation simulations were performed with our kinetic Monte Carlo stochastic MC-RRKM code,<sup>63</sup> used in our previous studies of similar systems, able to explicitly account for ISC among coupled portions of the PES. The code solves the 1D ME using  $k(E)$  RRKM rate constants determined from 2D  $k(E,J)$  rate parameters averaged over  $J$ , as suggested by Miller et al.<sup>64</sup> BF's were determined by counting the number of transitions to exit channels, which were treated in the simulations as irreversible sinks.<sup>65</sup> Further details are given in the SI.

## Data availability

The raw data underlying all the figures, as well as the full data needed to support, interpret, verify and extend the research in the article are available in its Supplementary Information, in the separated Source Data Files (that can be downloaded at <https://doi.org/10.6084/m9.figshare.20423616>), and also from the authors upon reasonable request.

## Methods-only references

- 44 Alagia, M. *et al.* Magnetic Analysis of Supersonic Beams of Atomic Oxygen, Nitrogen, and Chlorine Generated from a Radio-Frequency Discharge. *Isr. J. Chem.* **37**, 329-342 (1997).
- 45 Becke, A. D. Density-functional thermochemistry. III. The role of exact exchange. *J. Chem. Phys.* **98**, 5648-5652 (1993).
- 46 Grimme, S., Ehrlich, S. & Goerigk, L. Effect of the damping function in dispersion corrected density functional theory. *J. Comput. Chem.* **32**, 1456-1465 (2011).
- 47 Crehuet, R. & Bofill, J. M. The reaction path intrinsic reaction coordinate method and the Hamilton–Jacobi theory. *J. Chem. Phys.* **122**, 234105 (2005).
- 48 Papajak, E., Leverentz, H. R., Zheng, J. & Truhlar, D. G. Efficient Diffuse Basis Sets: cc-pVxZ+ and maug-cc-pVxZ. *J. Chem. Theory Comput.* **5**, 1197-1202 (2009).
- 49 Raghavachari, K., Trucks, G. W., Pople, J. A. & Head-Gordon, M. A fifth-order perturbation comparison of electron correlation theories. *Chem. Phys. Letts.* **157**, 479-483 (1989).

- 50 Møller, C., & Plesset, M. S. Note on an approximation treatment for many-electron systems. *Phys. Rev.* **46**, 618-622 (1934).
- 51 Peterson, K. A. & Dunning, T. H., Jr. Accurate correlation consistent basis sets for molecular core-valence correlation effects: The second-row atoms Al-Ar, and the first-row atoms B-Ne revisited. *J. Chem. Phys.* **117**, 10548–10560 (2002).
- 52 Lupi, J., Puzzarini, C., Cavallotti, C. & Barone, V. State-of-the-Art Quantum Chemistry Meets Variable Reaction Coordinate Transition State Theory to Solve the Puzzling Case of the H<sub>2</sub>S + Cl System. *J. Chem. Theory Comput.* **16**, 5090-5104 (2020).
- 53 Alessandrini, S., Tonolo, F. & Puzzarini, C. In search of phosphorus in astronomical environments: The reaction between the CP radical (X<sup>2</sup>Σ<sup>+</sup>) and methanimine. *J. Chem. Phys.* **154**, 054306 (2021).
- 54 Frisch, M. *et al.* Gaussian 16, Revision C.01. (2016).
- 55 Chai, J.-D. & Head-Gordon, M. Long-range corrected hybrid density functionals with damped atom-atom dispersion corrections. *Phys. Chem. Chem. Phys.* **10**, 6615-6620 (2008)
- 56 Krishnan, R., Binkley, J.S., Seeger, R. & Pople, J. A. Self-consistent molecular orbital methods. XX. A basis set for correlated wave functions. *J. Chem. Phys.* **72**, 650 (1980)
- 57 Cavallotti, C., Pelucchi, M., Georgievskii, Y. & Klippenstein, S. J. EStokTP: Electronic Structure to Temperature- and Pressure-Dependent Rate Constants—A Code for Automatically Predicting the Thermal Kinetics of Reactions. *J. Chem. Theory Comput.* **15**, 1122-1145 (2019).
- 58 Werner, H.-J. *et al.* MOLPRO, version 2020.2, a package of ab initio programs. See <http://www.molpro.net> (2010).
- 59 Harvey, J. N. & Aschi, M. Modelling spin-forbidden reactions: recombination of carbon monoxide with iron tetracarbonyl *Faraday Discuss.* **124**, 129-143 (2003).
- 60 Zener, C. Non-adiabatic crossing of energy levels. *Proc. R. Soc. Lond. A* **137**, 696-702 (1932).
- 61 Wittig, C. The Landau–Zener Formula. *J. Phys. Chem. B* **109**, 8428-8430 (2005).
- 62 Georgievskii, Y., Klippenstein, S. J. Transition State Theory for Multichannel Addition Reactions: Multifaceted Dividing Surfaces. *J. Phys. Chem. A* **107**, 9776–9781 (2003).
- 63 Barbato, A.; Seghi, C.; Cavallotti, C. An Ab Initio Rice-Ramsperger-Kassel-Marcus/Master Equation Investigation of SiH<sub>4</sub> Decomposition Kinetics Using a Kinetic Monte Carlo Approach. *J. Chem. Phys.* **130**, 074108-1-11 (2009).
- 64 Miller, J. A.; Klippenstein, S. J.; Raffy, C. Solution of some one-and two-dimensional master equation models for thermal dissociation: The dissociation of methane in the low-pressure limit. *J. Phys. Chem. A* **106**, 4904-4913 (2002).
- 65 Georgievskii, Y.; Miller, J. A.; Burke, M. P.; Klippenstein, S. J. Reformulation and Solution of the Master Equation for Multiple-Well Chemical Reactions, *J. Phys. Chem. A* **117**, 12146-12154 (2013).